so that Rho family signalling is almost exclusively confined to regulating contraction through modifying Ca^{2+} sensitivity in the cytosol. By contrast, in dedifferentiated synthetic VSMCs, the reduction in myocardin expression leads to a reduction in basal SRF activity and then to a loss of VSMC-specific contractile components. Under these conditions, MRTF-A expression is induced, at least in part, by the reduction in miR-1 also caused by diminished myocardin, and is sufficient to maintain the SRF activity necessary for cellular migration and proliferation. Because MRTF-A is shuttled between the cytosol and nucleus, where it activates SRF downstream of Rho family GTPase-actin signalling, in dedifferentiated VSMCs extracellular stimuli activating Rho GTPase signalling can substantively affect cellular proliferation and migration by modulating SRF activity (Medjkane *et al*, 2009; Olson and Nordheim, 2010). Loss or inhibition of MRTF-A reduced stimulus-induced cell migration and proliferation, making cells static (Figure 6J). This suggests that the reciprocal expression of MRTF-A and myocardin mediated by miR-1 regulates the plasticity of effectors downstream of Rho family signalling, thereby contributing to phenotypic modulation of VSMC during vascular remodelling.

In addition to the classical concept that dedifferentiated intimal VSMCs are derived from medial VSMCs, recent evidence raises the possibility that VSMC progenitor cells in the circulation or adventitia also contribute to intimal VSMCs (Sata *et al*, 2002; Hoglund *et al*, 2010). We have not addressed the role of MRTF-A in the process of intimal VSMC differentiation from such progenitor cells in this study. In that context, however, MRTF-A has been shown to be involved in the differentiation of mesenchymal stem cells into VSMCs (Jeon *et al*, 2008). Thus, MRTF-A may also play an important role in the molecular processes underlying migration, proliferation and differentiation of VSMC progenitor cells into intimal VSMCs during vascular remodelling.

Recently, human genetic screening to identify novel susceptibility loci for CAD using microsatellite markers and SNP analysis revealed that an SNP in the promoter region of the MRTF-A gene (−184C>T) is associated with susceptibility to CAD (Hinohara *et al*, 2009). Moreover, functional analysis suggested that heightened MRTF-A expression is associated with increased susceptibility to CAD. We observed that the MRTF-A promoter containing −184T, which is associated with high CAD susceptibility, showed significantly stronger transcriptional activity than the wild-type promoter in cultured VSMCs (Figure 6I). These observations further support the conclusion that MRTF-A is crucially involved in pathological vascular remodelling underlying the development of vascular diseases, and imply that MRTF-A is a potentially useful therapeutic target for prevention of the progression of vascular diseases.

Materials and methods

Plasmids

−930 bp MRTF-A(−184C)-luc (MRTF-A-luc), vinculin-luc, vinculin CArG-mut-luc and 3 × CArG-luc were described previously (Kuwahara *et al*, 2007; Morita *et al*, 2007; Hinohara *et al*, 2009). Expression vectors used in the experiments were described previously (Kuwahara *et al*, 2007). MRTF-A 3′UTR-luc and mutMRTF-A 3′UTR-luc were respectively generated by inserting the MRTF-A 3′UTR containing wild type or mutated miR-1 target sequences downstream of the luciferase gene in a pMIR-REPORTER kit miRNA reporter expression vector (Ambion). −5500 bp MRTF-A-luc was generated by inserting 5500 bp of the 5′-FR of MRTF-A gene upstream of the luciferase gene in pGL4 vector (Promega).

Animal experiments

MRTF-A$^{-/-}$ mice were kindly provided from Dr EN Olson (The University of Texas, Southwestern Medical Center at Dallas) (Li *et al*, 2006). *ApoE*$^{-/-}$ and *MRTF-A*$^{-/-}$ mice (C57BL/6 background) were cross-bred (Kobayashi *et al*, 2004; Li *et al*, 2006). The animal care and all experimental protocols were reviewed and approved by the Animal Research Committee at Kyoto University Graduate School of Medicine.

Cell culture and transfection

RAVSMCs (Cell Applications. Inc.), A7r5 (DS Pharma Biomedical), NIH3T3 and COS7 cells were maintained in DMEM supplemented with 10% FCS. Co-transfection of RAVSMCs with 3 × CArG-luc plus expression plasmids encoding MRTF-A (1 ng) and STARS (100 ng), or with MRTF-A-luc plus expression plasmids encoding myocardin and MRTF-A (0, 1 or 10 ng each) was accomplished using FuGene6 (Roche). pRL-TK (Roche) was included in all transfections as an internal control. MiRIDIAN microRNA mimic for miR-1, miRIDIAN microRNA hairpin inhibitor for miR-1 or a negative control for each (Thermo Scientific) was transfected into RAVSMCs grown in 6-cm dishes using Dharmafect2. MAVSMCs were obtained as previously reported (Nakamura *et al*, 2010).

RNA interference

RAVSMCs grown in 6-cm dishes were transfected with 200 pmol of ON-TARGET plus® siRNA reagent targeting rat MRTF-A or myocardin, or control scrambled siRNA (Thermo Scientific) using Dharmafect 2. For luciferase assays, RAVSMCs grown in 24-well dishes were transfected with 100 pmol of siRNA and 500 ng of luciferase reporter plasmid using Fugene 6.

Mouse vascular injury

Vascular wire injury was induced in femoral arteries of male C57BL/6 wild-type or *Mkl1*$^{-/-}$ mice at 8–10 weeks of age, as described previously (Sata *et al*, 2000; Takaoka *et al*, 2009). LNA oligonucleotide anti-miR-1 microRNA inhibitor or LNA microRNA inhibitor negative control (20 mg/kg) (5′-FAM prelabelled, Exiqon) was injected into sham-operated or injured femoral arteries from the muscular branch using a syringe with 29 gauge needle (TERUMO).

Quantification of neointimal hyperplasia

We harvested the femoral and carotid arteries 4 weeks after wire injury, unless otherwise indicated. Digitalized images were analysed using image analysis software (Image J, NIH), and the intimal and medial areas were recorded. The average of the neointima/media ratios in FIVE serial sections was designated as the value to represent each individual.

Analysis of atherosclerotic lesion area in *ApoE*$^{-/-}$ mice

Mkl1$^{+/+}$;*ApoE*$^{-/-}$ and *Mkl1A*$^{-/-}$;*ApoE*$^{-/-}$ mice were fed normal chow for 4 weeks beginning when the mice were 4 weeks old. Then beginning when they were 8 weeks old, they were fed a high-cholesterol diet (F2HFD1, Oriental Biotechnology) for 8 weeks. Atherosclerotic lesions were analysed by en-face analysis of the whole aorta and quantified by cross-sectional analysis of the proximal aorta, as described previously (Paigen *et al*, 1987; Palinski *et al*, 1994; Kobayashi *et al*, 2004).

Immunohistochemical analysis

Paraffin-embedded sections (4 μm thick) of femoral arteries harvested 4 weeks after wire injury were stained with anti-Mac3, anti-CD31, mouse monoclonal anti-αSMA (Sigma-Aldrich), rabbit polyclonal anti-SM-MHC (BT-562, Biomedical Technologies Inc.) or anti-BSAC antibodies (Sasazuki *et al*, 2002). Ratios of total numbers of Mac-3-positive cells in the intima and the media and CD31-positive endothelial cells in *Mkl1*$^{+/+}$ and *Mkl1*$^{-/-}$ mice were quantified ($n = 4$ and 5 in each group, respectively). Sections of proximal aortas from *ApoE*$^{-/-}$ mice were stained with anti-α-SMA, anti-SM-MHC or anti-BSAC antibody.

Real-time RT–PCR

Real-time one-step RT–PCR was performed using One-step RT-PCR master mix reagent (Applied Biosystems). MiR-1 expression was determined using a Taqman MicroRNA RT kit and Taqman Universal PCR Master Mix II (Applied Biosystems). All taqman primers and probes were purchased from Applied Biosystems.

Western blot analysis

Western blot analysis was performed using rabbit polyclonal anti-myocardin, anti-MRTF-A and anti-MRTF-B antibodies as described previously (Kuwahara *et al*, 2005; Nakamura *et al*, 2010).

Statistical analysis

Data are presented as means ± s.e.m. Unpaired *t*-tests were used for comparison between two groups, and ANOVA with *post hoc* Fisher's test was used for comparison among groups. Values of $P<0.05$ were considered as significant. Data obtained from the two-way factorial design were analysed with the two-way ANOVA.

Supplementary data

Supplementary data are available at *The EMBO Journal* Online (http://www.embojournal.org).

Acknowledgements

We thank H Yanagisawa (The University of Texas Southwestern Medical Center at Dallas), T Murayama, H Arai, E Ashihara and T Maekawa (Kyoto University) for their technical instruction; Y Kubo for her excellent secretarial work; K Hinohara (Tokyo Medical and Dental University) for preparation of MRTF-A-luciferase constructs; and F Kataoka, A Fujishima and A Abe for their excellent technical assistance. We also gratefully thank EN Olson and R Bassel-Duby (The University of Texas Southwestern Medical Center at Dallas) for providing us MRTF-A knockout mice. This research was supported by Grants-in-Aid for Scientific Research from the Japan Society for the Promotion of Science (to KK, AK and K N); a grant from the Japanese Ministry of Health, Labour and Welfare (to KN); grants from the Japan Foundation for Applied Enzymology, the Mitsubishi Pharma Research Foundation, the Astellas Foundation for Research on Metabolic Disorders, the Vehicle Racing Commemorative Foundation, the Takeda Medical Research Foundation, the Takeda Science Foundation, the Hoh-ansha Foundation, the SENSHIN Medical Research Foundation (to KK) and the Kimura Memorial Heart Foundation (to HK).

Author Contributions: TM conducted most of the experiments and contributed to data analysis. KK and NK conceived of and directed the project. MT, HK, YK, MS, TS and RN provided technical help on animal experiments. YN, HN, TN, KS and AK performed some experiments using luciferase reporter assays, immunohistochemical analysis and western blot analysis with TM. KN, YY, CY, JS, SU, TN and YK contributed to data analysis.

Conflict of interest

The authors declare that they have no conflict of interest.

References

Bentzon JF, Weile C, Sondergaard CS, Hindkjaer J, Kassem M, Falk E (2006) Smooth muscle cells in atherosclerosis originate from the local vessel wall and not circulating progenitor cells in ApoE knockout mice. *Arterioscler Thromb Vasc Biol* **26:** 2696–2702

Chen J, Yin H, Jiang Y, Radhakrishnan SK, Huang ZP, Li J, Shi Z, Kilsdonk EP, Gui Y, Wang DZ, Zheng XL (2011) Induction of microRNA-1 by myocardin in smooth muscle cells inhibits cell proliferation. *Arterioscler Thromb Vasc Biol* **31:** 368–375

Daniel JM, Bielenberg W, Stieger P, Weinert S, Tillmanns H, Sedding DG (2010) Time-course analysis on the differentiation of bone marrow-derived progenitor cells into smooth muscle cells during neointima formation. *Arterioscler Thromb Vasc Biol* **30:** 1890–1896

Evelyn CR, Wade SM, Wang Q, Wu M, Iniguez-Lluhi JA, Merajver SD, Neubig RR (2007) CCG-1423: a small-molecule inhibitor of RhoA transcriptional signaling. *Mol Cancer Ther* **6:** 2249–2260

Glass CK, Witztum JL (2001) Atherosclerosis. The road ahead. *Cell* **104:** 503–516

Hinohara K, Nakajima T, Yasunami M, Houda S, Sasaoka T, Yamamoto K, Lee BS, Shibata H, Tanaka-Takahashi Y, Takahashi M, Arimura T, Sato A, Naruse T, Ban J, Inoko H, Yamada Y, Sawabe M, Park JE, Izumi T, Kimura A (2009) Megakaryoblastic leukemia factor-1 gene in the susceptibility to coronary artery disease. *Hum Genet* **126:** 539–547

Hinson JS, Medlin MD, Lockman K, Taylor JM, Mack CP (2007) Smooth muscle cell-specific transcription is regulated by nuclear localization of the myocardin-related transcription factors. *Am J Physiol Heart Circ Physiol* **292:** H1170–H1180

Hoglund VJ, Dong XR, Majesky MW (2010) Neointima formation: a local affair. *Arterioscler Thromb Vasc Biol* **30:** 1877–1879

Jeon ES, Park WS, Lee MJ, Kim YM, Han J, Kim JH (2008) A Rho kinase/myocardin-related transcription factor-A-dependent mechanism underlies the sphingosylphosphorylcholine-induced differentiation of mesenchymal stem cells into contractile smooth muscle cells. *Circ Res* **103:** 635–642

Jiang Y, Yin H, Zheng XL (2010) MicroRNA-1 inhibits myocardin-induced contractility of human vascular smooth muscle cells. *J Cell Physiol* **225:** 506–511

Jin W, Goldfine AB, Boes T, Henry RR, Ciaraldi TP, Kim EY, Emecan M, Fitzpatrick C, Sen A, Shah A, Mun E, Vokes V, Schroeder J, Tatro E, Jimenez-Chillaron J, Patti ME (2011) Increased SRF transcriptional activity in human and mouse skeletal muscle is a signature of insulin resistance. *J Clin Invest* **121:** 918–929

Kenagy RD, Hart CE, Stetler-Stevenson WG, Clowes AW (1997) Primate smooth muscle cell migration from aortic explants is mediated by endogenous platelet-derived growth factor and basic fibroblast growth factor acting through matrix metalloproteinases 2 and 9. *Circulation* **96:** 3555–3560

Kobayashi T, Tahara Y, Matsumoto M, Iguchi M, Sano H, Murayama T, Arai H, Oida H, Yurugi-Kobayashi T, Yamashita JK, Katagiri H, Majima M, Yokode M, Kita T, Narumiya S (2004) Roles of thromboxane A(2) and prostacyclin in the development of atherosclerosis in apoE-deficient mice. *J Clin Invest* **114:** 784–794

Kuwahara K, Barrientos T, Pipes GC, Li S, Olson EN (2005) Muscle-specific signaling mechanism that links actin dynamics to serum response factor. *Mol Cell Biol* **25:** 3173–3181

Kuwahara K, Teg Pipes GC, McAnally J, Richardson JA, Hill JA, Bassel-Duby R, Olson EN (2007) Modulation of adverse cardiac remodeling by STARS, a mediator of MEF2 signaling and SRF activity. *J Clin Invest* **117:** 1324–1334

Li S, Chang S, Qi X, Richardson JA, Olson EN (2006) Requirement of a myocardin-related transcription factor for development of mammary myoepithelial cells. *Mol Cell Biol* **26:** 5797–5808

Li S, Wang DZ, Wang Z, Richardson JA, Olson EN (2003) The serum response factor coactivator myocardin is required for vascular smooth muscle development. *Proc Natl Acad Sci USA* **100:** 9366–9370

Liu Y, Sinha S, McDonald OG, Shang Y, Hoofnagle MH, Owens GK (2005) Kruppel-like factor 4 abrogates myocardin-induced activation of smooth muscle gene expression. *J Biol Chem* **280:** 9719–9727

Medjkane S, Perez-Sanchez C, Gaggioli C, Sahai E, Treisman R (2009) Myocardin-related transcription factors and SRF are required for cytoskeletal dynamics and experimental metastasis. *Nat Cell Biol* **11:** 257–268

Miano JM (2003) Serum response factor: toggling between disparate programs of gene expression. *J Mol Cell Cardiol* **35:** 577–593

Miralles F, Posern G, Zaromytidou AI, Treisman R (2003) Actin dynamics control SRF activity by regulation of its coactivator MAL. *Cell* **113:** 329–342

Morita T, Mayanagi T, Sobue K (2007) Reorganization of the actin cytoskeleton via transcriptional regulation of cytoskeletal/focal adhesion genes by myocardin-related transcription factors (MRTFs/MAL/MKLs). *Exp Cell Res* **313:** 3432–3445

Nakamura S, Hayashi K, Iwasaki K, Fujioka T, Egusa H, Yatani H, Sobue K (2010) Nuclear import mechanism for myocardin family

members and their correlation with vascular smooth muscle cell phenotype. *J Biol Chem* **285:** 37314–37323

Nishimura G, Manabe I, Tsushima K, Fujiu K, Oishi Y, Imai Y, Maemura K, Miyagishi M, Higashi Y, Kondoh H, Nagai R (2006) DeltaEF1 mediates TGF-beta signaling in vascular smooth muscle cell differentiation. *Dev Cell* **11:** 93–104

Olson EN, Nordheim A (2010) Linking actin dynamics and gene transcription to drive cellular motile functions. *Nat Rev Mol Cell Biol* **11:** 353–365

Owens GK, Kumar MS, Wamhoff BR (2004) Molecular regulation of vascular smooth muscle cell differentiation in development and disease. *Physiol Rev* **84:** 767–801

Paigen B, Morrow A, Holmes PA, Mitchell D, Williams RA (1987) Quantitative assessment of atherosclerotic lesions in mice. *Atherosclerosis* **68:** 231–240

Palinski W, Ord VA, Plump AS, Breslow JL, Steinberg D, Witztum JL (1994) ApoE-deficient mice are a model of lipoprotein oxidation in atherogenesis. Demonstration of oxidation-specific epitopes in lesions and high titers of autoantibodies to malondialdehyde-lysine in serum. *Arterioscler Thromb* **14:** 605–616

Sasazuki T, Sawada T, Sakon S, Kitamura T, Kishi T, Okazaki T, Katano M, Tanaka M, Watanabe M, Yagita H, Okumura K, Nakano H (2002) Identification of a novel transcriptional activator, BSAC, by a functional cloning to inhibit tumor necrosis factor-induced cell death. *J Biol Chem* **277:** 28853–28860

Sata M, Maejima Y, Adachi F, Fukino K, Saiura A, Sugiura S, Aoyagi T, Imai Y, Kurihara H, Kimura K, Omata M, Makuuchi M, Hirata Y, Nagai R (2000) A mouse model of vascular injury that induces rapid onset of medial cell apoptosis followed by reproducible neointimal hyperplasia. *J Mol Cell Cardiol* **32:** 2097–2104

Sata M, Saiura A, Kunisato A, Tojo A, Okada S, Tokuhisa T, Hirai H, Makuuchi M, Hirata Y, Nagai R (2002) Hematopoietic stem cells differentiate into vascular cells that participate in the pathogenesis of atherosclerosis. *Nat Med* **8:** 403–409

Schwartz SM, deBlois D, O'Brien ER (1995) The intima. Soil for atherosclerosis and restenosis. *Circ Res* **77:** 445–465

Shoji M, Sata M, Fukuda D, Tanaka K, Sato T, Iso Y, Shibata M, Suzuki H, Koba S, Geshi E, Katagiri T (2004) Temporal and spatial characterization of cellular constituents during neointimal hyperplasia after vascular injury: Potential contribution of bone-marrow-derived progenitors to arterial remodeling. *Cardiovasc Pathol* **13:** 306–312

Sun Y, Boyd K, Xu W, Ma J, Jackson CW, Fu A, Shillingford JM, Robinson GW, Hennighausen L, Hitzler JK, Ma Z, Morris SW (2006) Acute myeloid leukemia-associated Mkl1 (Mrtf-a) is a key regulator of mammary gland function. *Mol Cell Biol* **26:** 5809–5826

Takaoka M, Nagata D, Kihara S, Shimomura I, Kimura Y, Tabata Y, Saito Y, Nagai R, Sata M (2009) Periadventitial adipose tissue plays a critical role in vascular remodeling. *Circ Res* **105:** 906–911

Wang D, Chang PS, Wang Z, Sutherland L, Richardson JA, Small E, Krieg PA, Olson EN (2001) Activation of cardiac gene expression by myocardin, a transcriptional cofactor for serum response factor. *Cell* **105:** 851–862

Wang DZ, Li S, Hockemeyer D, Sutherland L, Wang Z, Schratt G, Richardson JA, Nordheim A, Olson EN (2002) Potentiation of serum response factor activity by a family of myocardin-related transcription factors. *Proc Natl Acad Sci USA* **99:** 14855–14860

Wang Z, Wang DZ, Pipes GC, Olson EN (2003) Myocardin is a master regulator of smooth muscle gene expression. *Proc Natl Acad Sci USA* **100:** 7129–7134

Watanabe N, Kurabayashi M, Shimomura Y, Kawai-Kowase K, Hoshino Y, Manabe I, Watanabe M, Aikawa M, Kuro-o M, Suzuki T, Yazaki Y, Nagai R (1999) BTEB2, a Kruppel-like transcription factor, regulates expression of the SMemb/Nonmuscle myosin heavy chain B (SMemb/NMHC-B) gene. *Circ Res* **85:** 182–191

Xu W, Baribault H, Adamson ED (1998) Vinculin knockout results in heart and brain defects during embryonic development. *Development* **125:** 327–337

Zhao Y, Samal E, Srivastava D (2005) Serum response factor regulates a muscle-specific microRNA that targets Hand2 during cardiogenesis. *Nature* **436:** 214–220

Development/Plasticity/Repair

Glucocorticoid Suppresses Dendritic Spine Development Mediated by Down-Regulation of Caldesmon Expression

Daisuke Tanokashira,[1]* Tsuyoshi Morita,[1]* Ken'ichiro Hayashi,[1]* Taira Mayanagi,[1,3] Kentaro Fukumoto,[1,3,4] Yoshiko Kubota,[3] Toshihide Yamashita,[2] and Kenji Sobue[1,3]

Departments of [1]Neuroscience and [2]Molecular Neuroscience, Graduate School of Medicine, Osaka University, Suita, Osaka 565-0871, Japan, [3]Department of Neuroscience, Institute for Biomedical Sciences, Iwate Medical University, Yahaba-cho, Shiwa-gun, Iwate 028-3694, Japan, and [4]Department of Neuropsychiatry, School of Medicine, Iwate Medical University, Morioka, Iwate, 020-8505, Japan

Glucocorticoids (GCs) mediate the effects of stress to cause structural plasticity in brain regions such as the hippocampus, including simplification of dendrites and shrinkage of dendritic spines. However, the molecular mechanics linking stress and GCs to these effects remain largely unclear. Here, we demonstrated that corticosterone (CORT) reduces the expression levels of caldesmon (CaD), causing dendritic spines to become vulnerable. CaD regulates cell motility by modulating the actin-myosin system and actin filament stability. In cultured rat hippocampal neurons, CaD localized to dendritic spines by binding to filamentous actin (F-actin), and CaD expression levels increased during spine development. CaD stabilized the F-actin dynamics in spines, thereby enlarging the spine heads, whereas CaD knockdown decreased the spine-head size via destabilization of the F-actin dynamics. CaD was also required for chemical LTP-induced actin stabilization. The CaD expression levels were markedly decreased by exposure to CORT mediated by suppression of serum response factor-dependent transcription. High CORT levels reduced both the spine-head size and F-actin stability similarly to CaD knockdown, and overexpressing CaD abolished the detrimental effect of CORT on dendritic spine development. These results indicate that CaD enlarges the spine-head size by stabilizing F-actin dynamics, and that CaD is a critical target in the GC-induced detrimental effects on dendritic spine development.

Introduction

Glucocorticoid (GC) hormones are principal stress mediators released from the adrenal gland in response to stressful events. Prolonged stress and chronic GC exposure produce abnormal behaviors in experimental animals and an increased risk of psychiatric disorders in humans (McEwen, 1999, 2005; Phillips et al., 2005; Becker et al., 2007). In animals, maternal stress during pregnancy increases GC levels not only in the mother but also in the fetus, leading to structural alterations in the developing brain and abnormal behaviors in adult offspring (Weinstock, 2008). In humans, prenatal stress is associated with increased anxiety in adolescence and a greater incidence of psychiatric disorders in adulthood (McEwen, 2005; Phillips et al., 2005; Becker et al., 2007). Antenatal GC therapy in humans has been shown to reduce both the convolution index and surface area of the cortex (Modi et al., 2001). Exposure to repeated stress and excessive GCs adversely affects neuronal architecture, causing dendritic branches to atrophy and reducing the density of dendritic spines and changing spine morphology (Watanabe et al., 1992; Magariños et al., 1996; Wellman, 2001; Radley et al., 2004, 2006; Liston and Gan, 2011). Thus, repeated exposure to stress-induced GCs results in alterations of neuronal architecture related to psychiatric disorders, but the precise molecular and cellular mechanisms of these alterations have been largely unclear.

Most excitatory synapses are located in the dendritic spines, which are small actin-rich protrusions that change shape from filopodia to stubby or mushroom-shaped spines during the course of neuron development (von Bohlen Und Halbach, 2009). Spine morphology and density are of importance as structural foundation in cognitive function and behavior (Dumitriu et al., 2010; Bloss et al., 2011). Actin filaments, a central component of dendritic spines, regulate the spine morphology, dynamics, and function (Hotulainen and Hoogenraad, 2010). In long-term potentiation (LTP), which is considered a cellular event for memory formation, the spine heads enlarge and synaptic connections are strengthened. Actin filament formation is tightly associated with the establishment of LTP (Lisman, 2003; Hotulainen and Hoogenraad, 2010). Thus, actin dynamics play an important role in synaptic development and plasticity. Although chronic stress and GC exposure are reported to impair synaptic development and plasticity (Radley et al., 2006; Liston and Gan, 2011), the molecular mechanisms of their association with actin dynamics remain poorly understood.

Received May 16, 2012; revised Aug. 1, 2012; accepted Aug. 21, 2012.

Author contributions: T. Morita, K.H., T.Y., and K.S. designed research; D.T., T. Morita, K.H., T. Mayanagi, K.F., and Y.K. performed research; D.T., T. Morita, K.H., and T. Mayanagi analyzed data; T. Morita and K.S. wrote the paper.

This work was supported by Grants-in-aid for Scientific Research 20240038 from the Japan Society for the Promotion of Science (to K.S.) and 23110510 from the Ministry of Education, Culture, Sports, Science and Technology (MEXT) (to K.S).

*D. T., T. Morita, and K. H. contributed equally to this work.

The authors declare no competing financial interests.

Correspondence should be addressed to Dr. Kenji Sobue, Department of Neuroscience, Institute for Biomedical Sciences, Iwate Medical University, 2-1-1 Nishitokuta, Yahaba-cho, Shiwa-gun, Iwate 028-3694, Japan. E-mail: ksobue@iwate-med.ac.jp.

DOI:10.1523/JNEUROSCI.2380-12.2012

 0270-6474/12/3214583-09$15.00/0

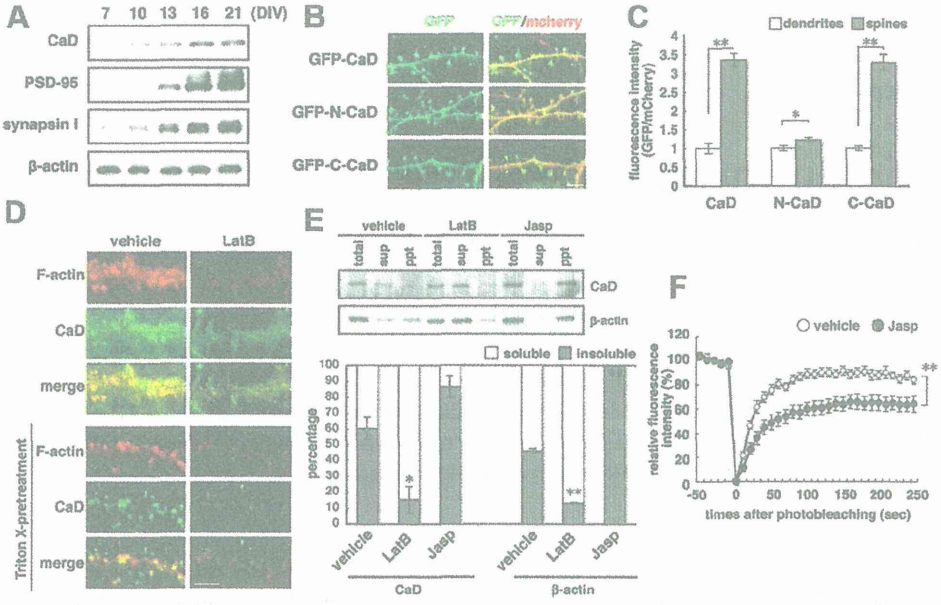

Figure 1. CaD expression profile and localization in developing hippocampal neurons. ***A***, CaD, PSD-95, and synapsin I protein expression profiles. ***B***, GFP-CaD, GFP-N-CaD, or GFP-C-CaD was exogenously expressed in neurons, using mCherry protein as a cell volume marker (scale bar, 5 μm). GFP and mCherry fluorescence intensities were measured in dendritic shafts and spines, respectively. ***C***, The graph shows GFP intensities corrected for mCherry intensities. CaD associates with F-actin ($^*p < 0.05$, $^{**}p < 0.01$). ***D***, Hippocampal neurons treated with DMSO (vehicle) or LatB for 3 h were incubated with (bottom) or without (top) 1% Triton X-100, then fixed and stained with anti-CaD antibody (green) and phalloidin (F-actin, red) (scale bar, 5 μm). ***E***, Neurons were treated with DMSO (vehicle), LatB, or Jasp, and then lysed with a solution containing Triton X-100. The lysates were separated into Triton X-soluble and -insoluble fractions by centrifugation. Western blotting was performed using equal load volumes of the fractions (top), and the CaD and β-actin proteins were quantified by densitometry (bottom). Data are means ± SE of values from three independent experiments ($^*p < 0.05$, $^{**}p < 0.01$). ***F***, GFP-CaD fluorescence recovery over time after photobleaching, measured in neurons treated with DMSO (vehicle) or jasplakinolide (Jasp). Data are means ± SE of values from 10 cells from three independent experiments ($^{**}p < 0.01$).

Caldesmon (CaD) is a ubiquitous actin-linked regulatory protein that binds to and stabilizes actin filaments (Sobue and Sellers, 1991; Mayanagi and Sobue, 2011). GCs affect expression level of CaD, which negatively controls the radial migration of neural progenitor cells by regulating actin-myosin interactions, leading to transiently retarded neocortical development (Fukumoto et al., 2009). CaD also regulates axon extension by inhibiting myosin II function (Morita et al., 2012). Thus, the CaD-mediated regulation of actin dynamics is important for brain development. However, the role of CaD in spine development is unclear. In this study we demonstrated that CaD stabilizes actin filaments and increases the head size of dendritic spines in hippocampal neurons, while GCs decrease CaD expression levels and cause the detrimental effects on spine development.

Materials and Methods

Antibodies. This study used the following purchased antibodies: anti-PSD-95 (MA1-045, Affinity BioReagents), anti-β-actin (A5441, Sigma), anti-SRF (sc-335, Santa Cruz Biotechnology), anti-GAPDH (FL-335, Santa Cruz Biotechnology), anti-GFP (A11120 and A11122, Invitrogen), and anti-DsRed (632496, Clontech). Anti-CaD and anti-synapsin1 antibodies were produced in rabbits.

Cell culture. Since the medium generally used to culture hippocampal neurons includes a B27 supplement containing an undisclosed concentration of CORT, we used CORT-free B27 supplement commissioned from Invitrogen and added CORT to the medium to reach defined concentrations. Hippocampal neurons were prepared from rats on embryonic day 18.5. Dispersed neurons were plated on poly-L-lysine-coated coverslips and cultured in glial-conditioned MEM containing 1 mM sodium pyruvate, 0.6% (W/V) D-glucose, and either 2% standard B27 supplement (Invitrogen) or 2% CORT-free B27 supplement with the indicated concentrations of CORT added. After 1 week, one-half of the medium was changed to neurobasal (Invitrogen) medium containing 0.5 mM L-glutamine (Sigma) with either 2% standard B27 supplement or 2% CORT-free B27 supplement with the indicated concentrations of CORT added, and the neurons were cultured for another 2 weeks. All experiments using the cultured rat hippocampal neurons were performed during 21–24 d *in vitro* (DIV). All animal experiments were performed in accordance with guidelines from the Osaka University School of Medicine and the Iwate Medical University.

Foot-shock stress. Male Wistar rats (9–10 weeks old) (Japan SLC) were housed under controlled 12 h/12 h light/dark (lights on at 7:00 A.M.) and temperature (23 ± 2°C) conditions. Rats were randomly allocated to stress or control groups, and rats in the stress group were subjected to a single session of foot shocks. Foot-shock stress was applied in a foot-shock box with a grid floor connected to a shock generator (Med Associates) controlled by FreezeFrame software (Actimetrics). During this session, the rats received four uncontrollable, inescapable foot shocks (current intensity, 1.0 mA; duration, 1.0 s at random intervals of 60–90 s). After the session, the rat remained in the chamber for 60 s and was then returned to its home cage.

Determination of CORT concentrations. To avoid the influence of time-related CORT fluctuations, all experiments using live rats were performed between 10:30 A.M. and 11:00 A.M. Rats were anesthetized and decapitated, and blood was collected from the heart. The blood plasma was collected by centrifugation. At the same time, the brain was quickly removed, and cerebral tissue samples were individually homogenized in ice-cold PBS using a Potter–Elvehjem homogenizer and an ultrasound sonicator. Tissue homogenates were centrifuged and the supernatants were collected. Blood plasma and brain extracts were immediately stored at −80°C. CORT concentrations in these samples were determined with the Corticosterone EIA Kit (YK240, Yanaihara), which directly determines CORT concentrations using specially formulated sample diluents that displace CORT-binding globulin (CBG).

Expression plasmids and transfection. The coding regions for human *l*-CaD and its N terminus (1–263 aa) and C terminus (264–558 aa) and for human β-actin were amplified by PCR and subcloned into the highly efficient mammalian expression plasmid pCAGGS. EGFP, mCherry, or the myc-tag sequence was fused to the 5′ end of the coding sequences.

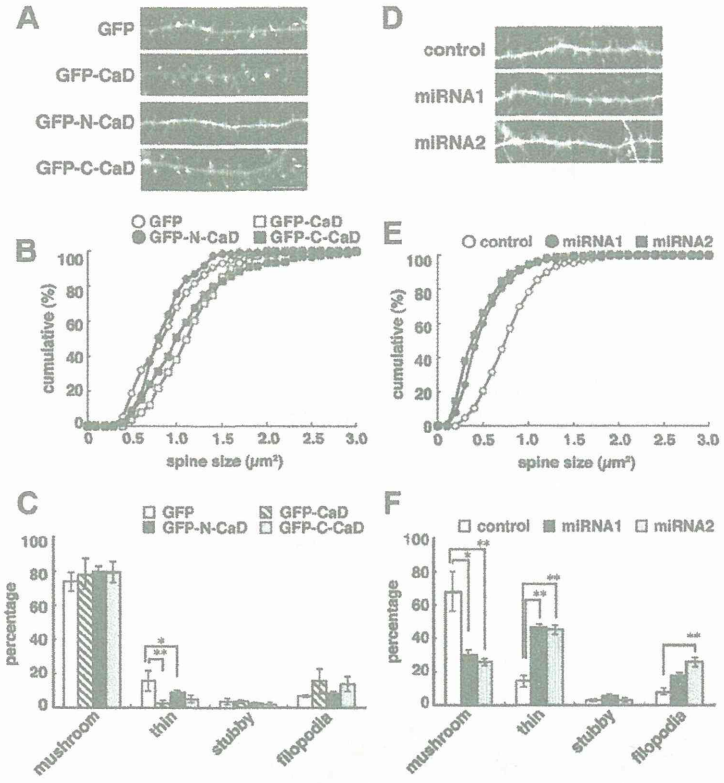

Figure 2. CaD regulates spine size in hippocampal neurons. *A*, Spine morphology in neurons transfected with GFP, GFP-CaD, GFP-N-CaD, or GFP-C-CaD (scale bar, 10 μm), and graphs of spine sizes and their cumulative distributions (*B*), and classification of spine morphology (*C*). *D*, Spine morphology in neurons transfected with control miRNA, CaD miRNA1, or CaD miRNA2 (scale bar, 10 μm), and graphs of spine sizes and their cumulative distributions (*E*), and classification of spine morphology (*F*).

The mCherry-LifeAct and miRNA plasmids were constructed as previously reported (target sequences: CaD miRNA1, GAGATGTATCTGGCAAGCGGA; CaD miRNA2, CTGGAGCAATATACCAATGCA) (Fukumoto et al., 2009; Morita et al., 2012). Hippocampal neurons were transfected by the calcium phosphate method as described previously (Jiang and Chen, 2006). Transfection was performed at 7 DIV (for miRNA) or 19 DIV (for CaD-overexpression).

Imaging. Neurons were cultured on coverslips, fixed using 4% paraformaldehyde, incubated with a primary antibody, and then incubated with the appropriate Alexa-labeled secondary antibody. To visualize filamentous actin (F-actin), Alexa 568-phalloidin (Invitrogen) was added in the secondary antibody solution. Stained neurons were observed under a BIOREVO BZ-9000 (Keyence) fluorescence microscope with an ×100 oil-immersion lens. Living neurons were cultured in a glass-bottom dish with Tyrode's solution (119 mM NaCl, 2.5 mM KCl, 25 mM HEPES, 30 mM glucose, 2 mM $CaCl_2$, and 2 mM $MgCl_2$, pH 7.4) and observed under an LSM5 PASCAL laser-scanning microscope (Carl Zeiss) with an ×63 oil-immersion lens.

To monitor actin turnover in dendritic spines, neurons transfected with GFP and mCherry-β-actin were analyzed by FRAP assay as previously described (Star et al., 2002). A high-intensity 543 nm He-Ne laser was used to bleach the mCherry fluorescence in single spines, and the fluorescence recovery was observed with a low-power laser every 10 s. GFP fluorescence was simultaneously detected with a 488 nm argon laser to monitor spine volume change. Actin turnover in the spine was evaluated by the fluorescence recovery of mCherry-β-actin, corrected for background and GFP intensity to avoid the influence of spine volume changes during observation. The GFP-CaD dynamics in spines were also analyzed by FRAP. Neurons were transfected with GFP-CaD and mCherry. The GFP-CaD fluorescence in a single spine was bleached and the fluorescence recovery was observed every 10 s. The GFP-CaD intensity was corrected for background and mCherry intensity. The FRAP curve was fit to the equation: $F(t) = 1 - f_s - f_f * \exp^{(-t/\lambda)}$ in the previous report (Star et al., 2002), where f_s, f_f, t, and λ are the stable fraction, dynamic fraction, time (second), and time constant, respectively. The time constant during fluorescence recovery was analyzed according to the equation for the first 60 s.

To monitor F-actin dynamics in dendritic spines, neurons were transfected with GFP and mCherry-LifeAct. Fluorescence was detected every 10 s. F-actin dynamics were evaluated by the average change rate per 10 s of mCherry intensity, corrected for background and EGFP intensity to avoid the influence of spine volume change during observation. Actin-depolymerizing drug, latrunculin B (LatB, 5 μM), and actin-stabilizing drug jasplakinolide (Jasp, 100 nM) were used in actin dynamics-targeted experiments.

Chemical LTP. Chemical LTP (cLTP) was induced in cultured hippocampal neurons as previously described (Otmakhov et al., 2004). Neurons were incubated for 15 min in Tyrode's solution containing 6 μM 2-chloroadenosine. The solution was replaced by $MgCl_2$-free Tyrode's solution containing 100 μM picrotoxin, 50 μM forskolin, and 0.1 μM rolipram, and the neurons were incubated for another 15 min. After cLTP was induced, the solution was washed out with normal Tyrode's solution. Neurons were observed 3 h after cLTP induction.

Triton X-100-insoluble cytoskeletons. Neurons were treated with BRB buffer (10 mM PIPES pH 7.4, 3 mM NaCl, 100 mM KCl, 3.5 mM $MgCl_2$, and 1.25 mM EGTA) containing 1% Triton X-100 and protease inhibitor cocktail (Takara) for 2 min and were then washed with Triton X-100-free BRB buffer. The neurons were fixed and stained with anti-CaD antibody and phalloidin. For sedimentation assays, neurons were lysed with BRB buffer containing Triton X-100, and the lysate was separated by ultracentrifugation at 100,000 × *g* for 2 h. The supernatant and pellet were subjected to Western blotting as the Triton X-soluble and -insoluble fractions, respectively.

Quantitative real-time PCR. Total RNA was extracted from neurons, and cDNA was synthesized using the High-Capacity cDNA Reverse Transcription Kit (Applied Biosystems); mRNA levels were quantified by real-time PCR (RT-PCR) using SYBR GreenER qPCR SuperMix (Invitrogen) and were normalized to GAPDH mRNA expression. The respective primers were designed and synthesized by Sigma as follows: Gapdh-F (forward): CTCCCATTCTTCCACCTTTGATG, Gapdh-R (reverse): CCACCACCCTGTTGCTGTAG; Cald1-F: ATGTGGGAGAAAGGGAGTGTG, Cald1-R: CTTGGGAGCGGGTGACTTG, Cald1-Fibrotype-F: CTTGCTGGGTTGCTTAAAGG, Cald1-HeLa-type-F: CAGCTGCGGACATGCTTAG, Cald1-common-R: CTGTCACCTGTCCCAAGGAT; β-actin-F: CGTTGACATCCGTAAAGACCTC, β-actin-R: ATAGAGCCACCAATCCACACAG; PSD-95-F: CAGTGAGACCGACGACATTGG, PSD-95-R: ATGATGATGGGACGAGCATAGTG.

Reporter assays. The reporter constructs for the fibroblast-type promoter region of the rat *CALD1* gene were described previously (Fukumoto et al., 2009). The cells were lysed with Passive Lysis buffer (Promega), and the luciferase and β-galactosidase activities were measured using the luciferase assay system (Promega) and luminescent β-galactosidase detection kit II (Clontech), respectively.

Data quantification and statistics. Data from Western analysis were quantified by densitometry using ImageJ software. Data from synapse imaging were quantified using MetaMorph (Molecular Devices), BZ-II analysis application (Keyence; for fixed-cell imaging) or LSM5 PASCAL (Carl Zeiss; for live-cell imaging). All experiments were performed at

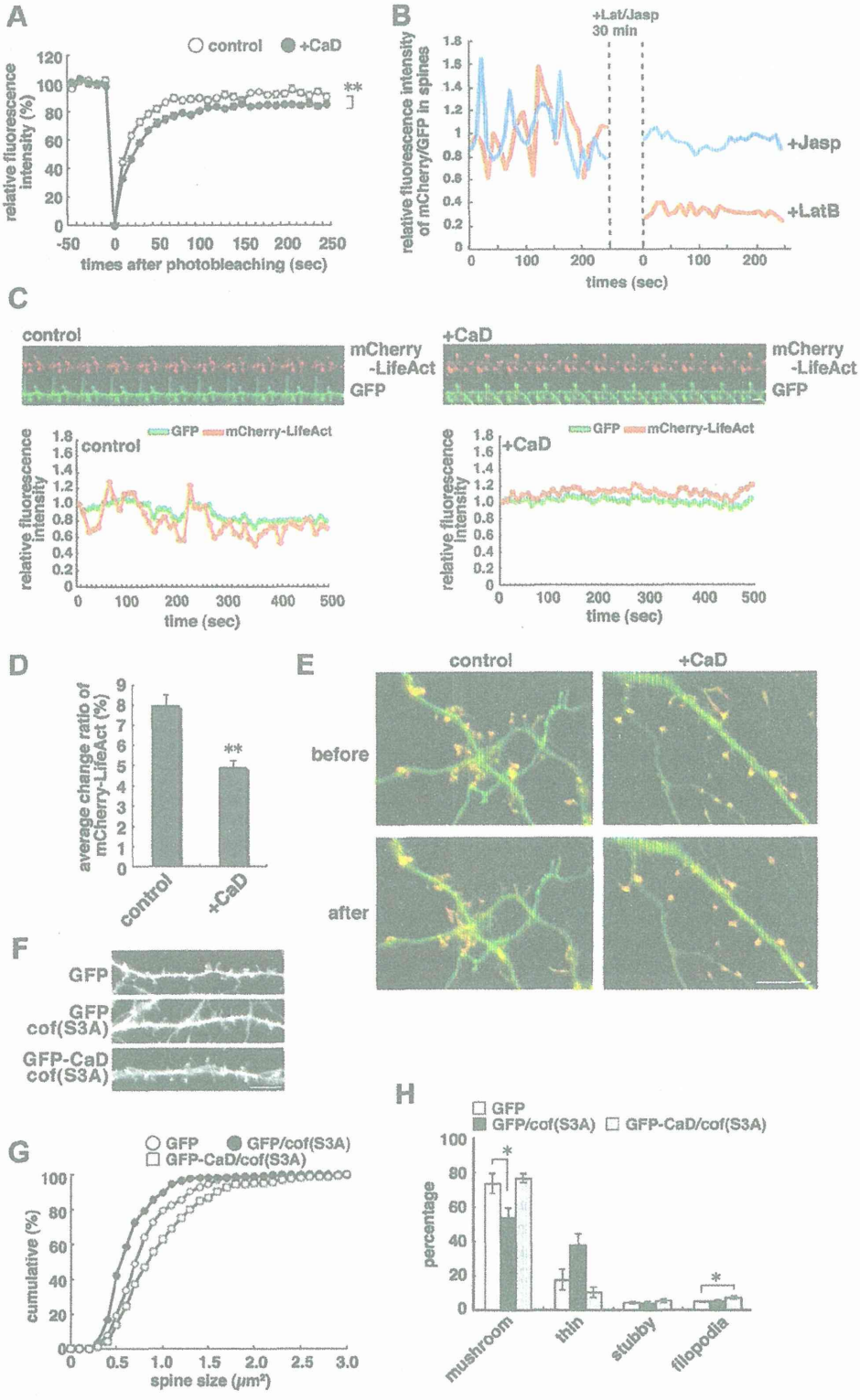

Figure 3. CaD effect on actin dynamics. ***A***, The fluorescence recovery of mCherry-β-actin over time after photobleaching, measured in neurons transfected with a mock vector (control) or myc-tagged-CaD (+CaD). Data are means ± SE of values from 10 cells (**$p < 0.01$). ***B***, Hippocampal neurons were transfected with GFP and mCherry-LifeAct to visualize spine volume changes and F-actin dynamics. The neurons were treated with Jasp or LatB for 30 min in the middle of the observation period, and changes in the mCherry and GFP fluorescence intensities in the spines were measured. The graph shows F-actin dynamics, corrected for the spine volume change (mCherry/GFP). F-actin dynamics were suppressed at high Jasp or low LatB levels; these agents elicit F-actin stabilization and depolymerization, respectively. ***C***, Neurons were transfected with GFP, mCherry-LifeAct, and either a mock vector (control) or myc-CaD (+CaD). Changes in fluorescence intensities in spines, observed every 10 s (top) (scale bar, 2 μm), are shown in the graph (bottom). Compared with GFP intensity changes, the mCherry intensity fluctuated dramatically in control neurons, whereas both the GFP and mCherry intensities were relatively stable in CaD-transfected neurons. ***D***, Spine F-actin dynamics, observed with mCherry-LifeAct. The graph shows change rates of mCherry-LifeAct fluorescence intensity in spines. Data are means ± SE of values from at least 18 spines (**$p < 0.01$). ***E***, Neurons were transfected with GFP and mCherry-LifeAct to visualize the spine shape and the F-actin activity, and F-actin accumulation in spines was observed before or after LatB treatment. Scale bar, 10 μm. ***F***, Spine morphology in neurons transfected (*Figure legend continues.*)

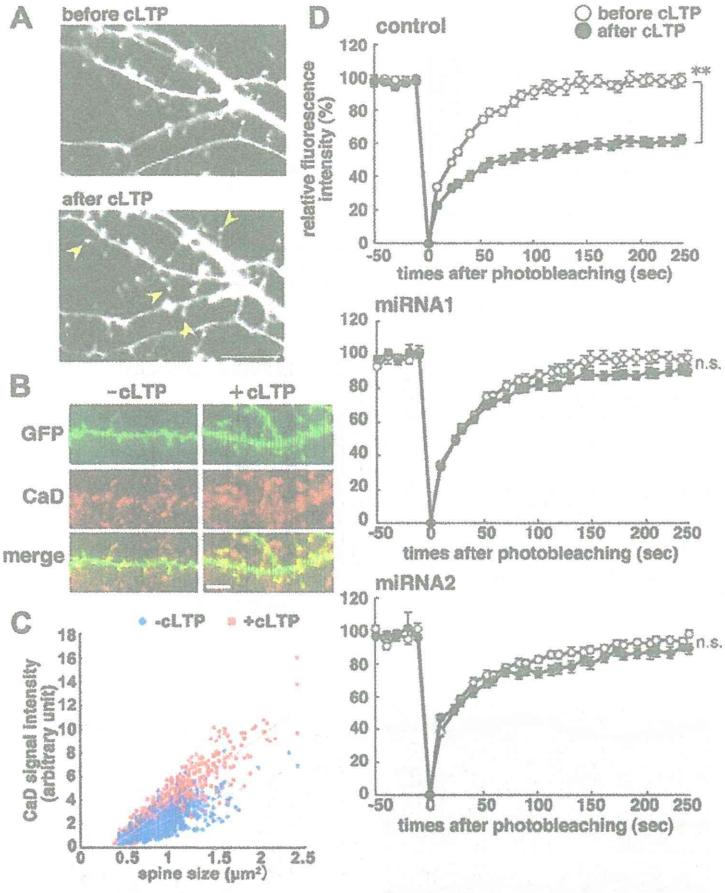

Figure 4. CaD is necessary for chemical LTP to induce F-actin stabilization in spines. *A*, Spine morphology before and after cLTP; yellow arrowheads indicate enlarged spines after cLTP (scale bar, 10 μm). *B*, CaD accumulation in enlarged spines after cLTP (scale bar, 5 μm). *C*, Scatter plot of spine sizes versus CaD intensities in each spine in neurons with (red square) or without cLTP (blue diamond). Data are obtained from at least 727 spines ($p < 0.01$). *D*, Fluorescence recovery of mCherry-β-actin over time after photobleaching, in hippocampal neurons transfected with control miRNA, CaD miRNA1, or CaD miRNA2. FRAP assays were performed before and after cLTP. Data are means ± SE of values from at least 10 cells (**$p < 0.01$).

least three times independently. Statistical significance was evaluated by classical Student's *t* test, paired *t* test, or one-way ANOVA.

Results

CaD accumulates in spines

CaD levels increased during development of rat hippocampal neurons in culture and reached a peak at 16–21 d *in vitro* (DIV), concurrent with dramatic increases in the postsynaptic protein PSD-95 and the presynaptic protein synapsin I (Fig. 1*A*). GFP-tagged full-length CaD (GFP-CaD) exogenously expressed in the neurons appeared to accumulate in spines (Fig. 1*B*). The CaD (GFP-C-CaD) C-terminal fragment, which includes actin-binding domains, was also localized to spines, while the N-terminal fragment (GFP-N-CaD), which lacks actin-binding ability, was dispersed through both dendrites and spines (Fig. 1*B*,*C*). These results suggest that CaD accumulates in spines by associating with F-actin via its actin-binding domains. Consistent with this scenario, endogenous CaD was localized in the spines and was resistant to Triton X-100 treatment (Fig. 1*D*, left). The Triton X-100 resistance was abolished by the F-actin-depolymerizing agent latrunculin B (LatB) (Fig. 1*D*, right). In sedimentation assays, ~60% of the CaD protein cosedimented with β-actin in the Triton X-100-insoluble fraction, and LatB treatment shifted their localization to the soluble fraction (Fig. 1*E*). After treatment with the actin-polymerizing agent jasplakinolide (Jasp), >80% of the CaD and β-actin cosedimented in the insoluble fraction (Fig. 1*E*). Fluorescence recovery after photobleaching (FRAP) assay also revealed that Jasp treatment reduced the GFP-CaD turnover rate in spines (Fig. 1*F*). These data demonstrate that CaD is actively accumulated into spines through its association with F-actin.

CaD enlarges the spine heads by stabilizing actin filaments

To determine the function of CaD in spine dynamics, we overexpressed the CaD fragments in neurons. While GFP-CaD or GFP-C-CaD induced larger spine heads than GFP did alone, GFP-N-CaD did not (Fig. 2*A–C*). We also depleted endogenous CaD using plasmid-type miRNA expression vectors, which were validated in previous studies (Fukumoto et al., 2009; Morita et al., 2012). Depleting endogenous CaD markedly reduced the spine-head size and changed the spine shape from mushroom to thin or filopodial (Fig. 2*D–F*). FRAP assay using mCherry-β-actin revealed that exogenous CaD significantly reduced the actin turnover rate within spines (Fig. 3*A*). The time constants (inverse of the turnover rate) for actin turnover were 19.3 ± 1.1 s in GFP-transfected neurons versus 24.6 ± 0.9 s in GFP-CaD-transfected neurons ($p < 0.01$). These data indicated that F-actin was stabilized. We also measured F-actin dynamics using mCherry-LifeAct, which selectively binds to F-actin and demonstrated real-time changes in the amount of F-actin within spines (Fig. 3*B*). The dendritic spines exhibit spontaneous motility as previously reported (Fischer et al., 1998, 2000; Korkotian and Segal, 2001; Star et al., 2002), and the dynamic motility is crucially based on the actin cytoskeleton (Fischer et al., 1998; Star et al., 2002). In control neurons, the amount of F-actin in spines varied dramatically compared with the spine volume traced by GFP (Fig. 3*C*). F-actin localization in CaD-transfected spines was more stable than that in control spines (Fig. 3*C*,*D*). This localization was resistant to LatB treatment (Fig. 3*E*), implicating that CaD stabilizes F-actin turnover in spines. Cofilin is considered to be a main factor for F-actin depolymerization and severing in spines (Lisman, 2003; Sarmiere and Bamburg, 2004). Indeed, cof(3A) (constitutively active cofilin) reduced the spine-head size (Fig. 3*F*, *G*). Interestingly, GFP-CaD protected F-actin from cof(3A) attack and thus promoted mushroom-shaped spines (Fig. 3*F–H*). Together, these results indicate that CaD stabilizes actin filaments in spines, leading to larger spine heads.

←

(*Figure legend continued.*) with GFP, GFP-CaD, and/or cof(S3A) (scale bar, 10 μm); the graph shows spine sizes and their cumulative distributions (*G*) and classification of spine morphology (*H*). Dendritic protrusions in the neurons were classified by morphology: mushroom, thin, stubby, or filopodial. Data are means ± SE of values from at least 147 spines.

CaD is necessary for chemical LTP to induce F-actin stabilization in spines

Actin filament stabilization is tightly linked to LTP-induced spine-head enlargement (Lisman, 2003; Hotulainen and Hoogenraad). In cultured hippocampal neurons, cLTP triggered to enlarge spine heads (Fig. 4*A*) and to accumulate endogenous CaD into the enlarged spine heads (Fig. 4*B*,*C*), suggesting that accumulated CaD contributes to stabilizing actin filament in the spines. FRAP assay confirmed that cLTP-induced spine head enlargement was associated with F-actin stabilization (Fig. 4*A*,*D*). In CaD-knockdown neurons, however, cLTP treatment did not stabilize F-actin (Fig. 4*D*). These results strongly suggest that CaD is critical for cLTP-induced F-actin stabilization in spine head enlargement.

CORT decreases CaD expression levels

We previously identified that CaD is one of the main downstream molecules in the GC-induced detrimental effects on the radial migration of neural progenitor cells during neocortical development (Fukumoto et al., 2009). Numerous studies have reported stress-induced increase in GC concentrations in the blood plasma or serum. However, GC concentration in the brain under nonstressed and stressed conditions remained unclear. Under conventional culture conditions without serum, neurons are, therefore, cultured in medium containing GC at nonstressed blood concentrations. To examine how GCs affect dendritic spine formation in cultured hippocampal neurons, we first examined the concentration of corticosterone (CORT), the principal GC in many species including rodents, in rat blood plasma and brain extracts after foot-shock stress. The CORT concentration increased markedly after stress, from 77.9 ± 30.0 nM to 1577.8 ± 191.6 nM ($p < 0.01$) in the blood plasma and from 16.7 ± 0.5 nM to 275.0 ± 36.0 nM ($p < 0.01$) in the brain (Fig. 5*A*). To culture hippocampal neurons with these CORT concentrations, our culture medium was prepared using CORT-free B27 supplement, with CORT added to defined concentrations. Importantly, the CaD levels decreased markedly according to the CORT dosage (Fig. 5*B–E*), and the F-actin was simultaneously decreased in spines (Fig. 5*D*, bottom). Thus, these results suggest that chronic CORT treatment decreases the localization of F-actin as well as CaD in spines, leading to the reduction of spine head size.

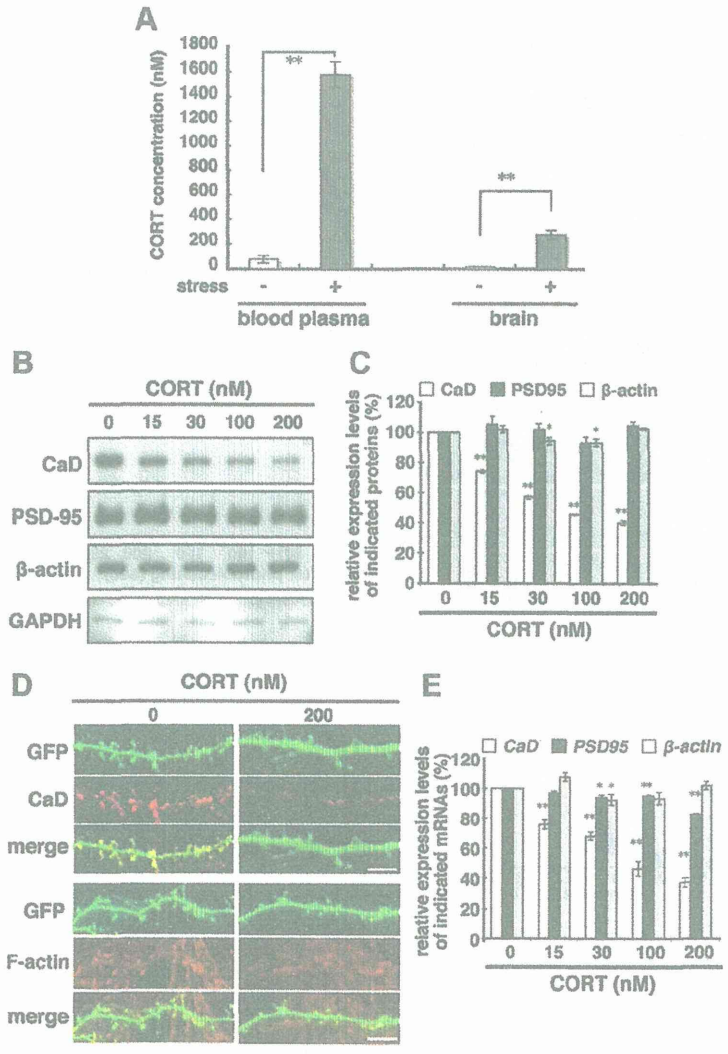

Figure 5. CORT decreases CaD expression. ***A***, A graph of CORT concentrations in blood plasma and brain extract; stress-induced CORT concentrations were measured shortly after rats received four uncontrollable, inescapable foot shocks. Data are means ± SE of values from three independent experiments (**$p < 0.01$). ***B***, CORT dose-dependent effects on CaD, PSD-95, and β-actin protein levels in neurons. Neurons were cultured with the indicated concentrations of CORT throughout the culture and prepared samples at 21–24 DIV. ***C***, Immunoblots shown in ***B*** were quantified by densitometry. Data are means ± SE of values from three independent experiments (*$p < 0.05$, **$p < 0.01$). ***D***, GFP-transfected neurons cultured with 0 or 200 nM CORT were fixed and stained with anti-GFP and anti-CaD antibodies (scale bar, 10 μm). ***E***, CORT dose-dependent effects on *CaD*, *PSD-95*, and β-actin mRNA levels, determined by RT-PCR. Data are means ± SE of values from three independent experiments (*$p < 0.05$, **$p < 0.01$).

We previously reported that the CaD gene encodes multiple isoforms, and that the fibro- and HeLa-type promoter regions, which function independently, regulate their transcription (Yano et al., 1994). In hippocampal neurons, CORT treatment suppressed the fibro-type isoforms more severely than the HeLa-type isoforms (Fig. 6*A*). Reporter assays showed that CORT reduced the CaD fibro-type promoter activity (Fig. 6*B*). The CaD promoter contains two putative *cis*-elements: a serum response factor (SRF)-binding CArG-box and a positive glucocorticoid receptor (GR)-binding glucocorticoid-responsive element (GRE)-like sequence (Mayanagi et al., 2008). In hippocampal neurons, the positive GRE-like sequence was not involved in CaD promoter activity, whereas a CArG-box mutation reduced the CaD promoter basal activity; CORT treatment did not produce any additional effect on this activity (Fig. 6*B*). These results suggest that CaD transcription was promoted by the SRF/CArG-box and was reduced by CORT through inhibition of the SRF/CArG-box-dependent transcription.

CORT prevents spine development by downregulating CaD

Consistent with the decrease in CaD and F-actin contents, CORT treatment resulted in smaller spine heads and a larger proportion of thin spines. At CORT levels of 100–200 nM, as found in the rat

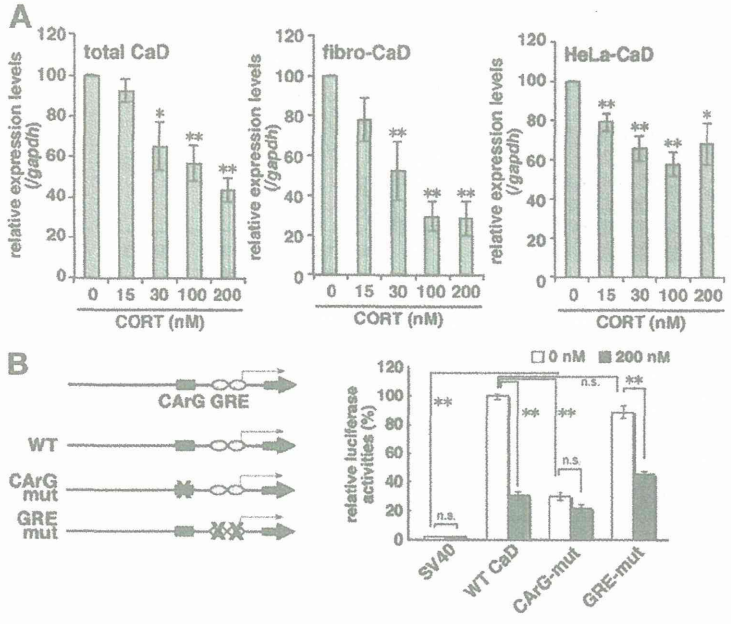

Figure 6. CORT effects on CaD isoform levels. *A*, Hippocampal neurons were cultured with CORT at the indicated concentrations. Total RNA was extracted, and RT-PCR was performed using specific primers for total CaD, fibro-type CaD, and HeLa-type CaD. Data are means ± SE of values from five independent experiments (*$p < 0.05$, **$p < 0.01$). *B*, A schematic diagram of mutation constructs of the CArG-box or GRE-like sequences in the rat fibro-type CaD promoter. Reporter assays were performed in hippocampal neurons (21–23 DIV) cultured with 0 or 200 nM CORT using the indicated promoter constructs. Reporter plasmid containing SV40 promoter (pGL3promoter) was used as a control. Data are means ± SE of values from three independent experiments (**$p < 0.01$).

brain under stress conditions, thin spines predominated with a corresponding decrease in the number of mushroom spines (Fig. 7*A–C*). FRAP assay demonstrated that CORT increased actin turnover rate (Fig. 7*D*). The time constants for actin turnover were 19.1 ± 0.7 s in the neurons cultured with 200 nM CORT compared with 28.6 ± 0.6 s in those cultured without CORT ($p < 0.01$). LifeAct assay also showed that CORT reduced the spine F-actin stability (Fig. 7*E*). As many actin-regulating proteins have been reported to modify spine shape, head size, and function (Lisman, 2003), we used RT-PCR to examine the expression of 25 actin-regulating genes. While CORT treatment affected the expression of some of these genes to a degree (data not shown), only CaD expression was markedly decreased (Fig. 5*B–E*). To confirm the importance of CaD reduction in the detrimental effect of CORT on dendritic spine development, we overexpressed CaD under high CORT concentrations. Exogenous CaD enlarged the spine-head size and promoted mushroom-shape spines even in the presence of 200 nM CORT (Fig. 8*A–C*). The spine F-actin stability that was reduced by CORT treatment was recovered by exogenous CaD (Fig. 8*D,E*). Both FRAP and LifeAct assays showed that exogenous CaD stabilized F-actin even under 200 nM CORT treatment [time constants in FRAP for CORT-treated spines: 17.8 ± 0.9 s vs for GFP-CaD-transfected CORT-treated spines: 28.0 ± 0.8 s ($p < 0.01$)]. These results suggest that CaD is a critical downstream player in the detrimental effects of CORT on actin cytoskeleton-dependent development of dendritic spines.

Discussion

In this study, we demonstrated that CaD modulates the spine-head size in cultured hippocampal neurons by regulating F-actin dynamics. CaD inhibits actin-myosin interactions and potently stabilizes F-actin (Sobue and Sellers, 1991; Mayanagi and Sobue, 2011). In hippocampal neurons, CaD was accumulated in spines via an interaction with F-actin (Fig. 1*B*), indicating that the function of CaD in spines depends on actin. Both full-length CaD and the CaD C-terminal fragment stabilized F-actin and increased the spine-head size (Fig. 2). Chemical LTP induction requires reorganization of the actin cytoskeleton, which shifts the G/F-actin ratio toward stable F-actin and increases the spine-head size (Gu et al., 2010). CaD was accumulated in spine heads in response to cLTP and stabilized the actin dynamics (Fig. 4). These results indicated that CaD was integral to this actin reorganization in spines (Figs. 2–4). Thus, F-actin dynamics regulated by CaD is critically involved in spine development and plasticity. Because CaD localization at spine heads also depends on F-actin, cooperative bidirectional interactions between CaD and F-actin may be ultimately required for regulating spine stability.

Neuronal architectures such as dendritic arborization and synaptic structure have plasticity in response to various factors, and this structural remodeling occurs throughout the lifespan (Dumitriu et al., 2010; McEwen, 2010; Liston and Gan, 2011; Bloss et al., 2011). These alterations correlate with cognitive and behavioral functions (Dumitriu et al., 2010; Bloss et al., 2011). Although transient stress exposure evokes adaptive responses of the hypothalamus-pituitary-adrenal (HPA)-axis, repeated or chronic stress causes the hyperactivation of this cascade. GCs have been intensely studied as a principal stress mediator. Exposure to high GCs triggers adverse effects on synapse formation, dendritic arborization, and hippocampal volume (Watanabe et al., 1992; Magariños et al., 1996; McEwen, 1999, 2005; Wellman, 2001; Radley et al., 2004; Radley et al., 2006; Liston and Gan, 2011). However, the molecular mechanisms are not fully understood. To examine the effects of GCs on cultured hippocampal neurons, we first measured the actual CORT concentrations in the blood plasma and brain of rats with or without foot-shock stress. Unexpectedly, the CORT concentrations in the brain were fivefold lower than those in the blood plasma, but they increased 16-fold after foot-shock stress (Fig. 5*A*). To test the effect of CORT levels on hippocampal neurons, we used a culture medium with a CORT-free B27 supplement and added CORT to defined concentrations. Using this culture system, we demonstrated that CORT at physiological concentrations inhibited dendritic spine development (Fig. 7*A–C*). F-actin dynamics are strongly linked to spine shape, motility, and plasticity (Hotulainen and Hoogenraad, 2010). CORT treatment destabilized the spine F-actin dynamics, changing the spine morphology from a mature mushroom shape to premature, thin, and filopodial shapes, as well as decreasing the spine-head size (Fig. 7). These data provide a novel insight regarding CORT-induced spine shrinkage as well as suppression of synapse formation and maturation. Previous *in vivo* histological studies have shown that chronic stress exposure decrease the number of dendritic spines (Radley et al., 2006). In addition, Liston and Gan